

Fourier Model Fitting for Vibration Analysis of Car Wheel Suspension Enhanced Damping System

Oleg Lyashuk^{1,†}, Mykola Stashkiv^{1,*,†}, Yurii Palianytsia^{1,†}, Roman Khoroshun^{1,†} and Dmytro Mironov^{1,†}

¹ Ternopil Ivan Puluj National Technical University, 56 Ruska Street, Ternopil, 46001, Ukraine

Abstract

This article presents a mathematical framework for analyzing vibration data from an enhanced damping system for car wheel suspension using Fourier series representations. The Fourier model fitting approach allows for decomposing the vibration signal into its constituent harmonic components, enabling a comprehensive understanding of the system's dynamic behavior. The methodology involves calculating the Fourier coefficients from the experimental data and reconstructing the signal using a truncated Fourier series representation. The article discusses the theoretical background, mathematical formulations, and practical implementation aspects of the Fourier model fitting technique, including preprocessing steps, coefficient estimation, and model validation. The proposed approach is illustrated with simulated and experimental data, demonstrating its effectiveness in characterizing the vibration patterns and identifying the dominant frequencies associated with the suspension system's performance.

Keywords

wheeled vehicle, controlled suspension, vibrations, information technologies, signal processing, Fourier model, computer modeling

1. Introduction


Over the past few decades, there has been a rapid development of the automotive industry in developed countries, a trend that is predicted to continue in the future. Unfortunately, Ukraine lags significantly behind in this development due to various factors such as war, corruption in government, lack of favorable legislation, lack of investment in the industry, and so on. However, according to experts' estimates, the potential benefit from investing in the transport industry for the domestic economy is around 8-10 billion dollars per year. Prior to the war, the transport sector, terminal and warehouse activities, and postal and courier services accounted for about 7% of GDP and 6% of employment among the working population in Ukraine.

*ITTAP'2024: 4th International Workshop on Information Technologies: Theoretical and Applied Problems, October 23-25, 2024, Ternopil, Ukraine, Opole, Poland

¹ Corresponding author.

[†] These authors contributed equally.

✉ oleglyashuk@ukr.net (O. Lyashuk); stashkiv@tntu.edu.ua (M. Stashkiv); palanizayb@tntu.edu.ua (Y. Palianytsia); horochunrt@gmail.com (R. Khoroshun); mironov.epz@gmail.com (D. Mironov)

 0000-0003-4881-8568 (O. Lyashuk); 0000-0002-7325-8016 (M. Stashkiv); 0000-0002-8710-953X (Y. Palianytsia); 0000-0002-1862-7640 (R. Khoroshun); 0000-0002-5717-4322 (D. Mironov)



© 2023 Copyright for this paper by its authors. Use permitted under Creative Commons License Attribution 4.0 International (CC BY 4.0).

This requires significant development and wide application of information modeling technologies for the impact of operating factors on the functioning of vehicles. The suspension system plays a crucial role in a wheeled vehicle design for its effective operation, as the longevity and efficiency of many of the vehicle systems depend on its reliable functioning. Taking into account all the above mentioned, it is reasonable to focus efforts on researching the impact of operating factors on the functioning of suspension systems in wheeled vehicles using information technologies.

To improve the smoothness of motion of wheeled vehicles (WV), controlled suspension systems are widely used [1]. In this paper a hybrid suspension system is proposed which combines the simplicity of the passive dampers with the performance of an electromagnetic active suspension. With a passive damper, it is possible to keep the performance of the active suspension, but using a smaller electromagnetic actuator [2]. The paper [3] describes experiments were carried out on a physical quarter car test rig with hardware-in-the-loop simulation (HILS) feature that fully incorporates the theoretical elements. In this paper [4], two different air spring models (classic air spring; dynamic air spring model) are presented. Thereafter, both the dynamic air spring suspension and the passive suspension are compared in terms of RMS of body acceleration, suspension travel, and dynamic tire force.

The fundamentals of researching the dynamics of vehicles, which is an important part of both classical [5, 6] and modern automobile theory, were laid down in the following articles [7, 8]. It is known that controlled suspension systems are widely used on wheeled chassis to improve the smoothness of motion of vehicles [9] and dynamic steering varies its degree of implementation up depending on driving speed, steering angle, and the mode selected in the dynamic handling system [10]. In [11, 12] optimal control algorithm for the semi-active suspension of the developed using a linear quadratic Gaussian. In the simulation, a hydro-pneumatic suspension system model is developed using SimulationX and is applied to a full vehicle model using MATLAB/Simulink [13, 14, 15, 16]. This [17, 18] paper synthesizes an adaptive tracking control strategy for vehicle suspension systems to achieve suspension performance improvements. The proposed control algorithm is formulated by developing a unified framework of non-ideal actuators rather.

The basics of studying the dynamics of vehicles, which are an important part of both classical [19] and modern theory of automobiles, have been laid out in the articles [9]. In the article [20] applied RMS optimization method is based on minimizing the absolute acceleration root mean square (RMS) with respect to the relative displacement RMS. The result of RMS optimization introduces an optimal design curve for a fixed mass ratio.

In the articles [21, 22], some vibrations of wheeled vehicles caused by road roughness, which affects the smoothness of vehicle travel, have been thoroughly examined. The methods and results of experimental studies on the smoothness of travel, maneuverability, and stability of motion of multi-axle wheeled vehicles, as well as the determination of system parameters and characteristics, have been described in the articles [23]. Some methods for improving the vibration protection properties of suspensions of different wheeled vehicles on a wheelbase using pneumatic, hydropneumatic springs, and hydraulic shock absorbers with self-regulating characteristics (due to vibration energy) have been presented in the articles [24, 25, 26].

Vibration analysis is a crucial aspect in the design and optimization of automotive suspension systems. An enhanced damping system for car wheel suspension aims to improve ride comfort and handling by effectively dissipating unwanted vibrations induced by road

irregularities and vehicle dynamics. To evaluate the performance of such a system, it is essential to analyze the vibration data collected from various sensors mounted on the suspension components.

One powerful technique for vibration analysis is the Fourier series representation, which decomposes a periodic signal into a sum of sinusoidal components with different frequencies, amplitudes, and phases. By fitting a Fourier model to the experimental data, it becomes possible to identify the dominant frequencies contributing to the overall vibration pattern, as well as their respective amplitudes and phases.

This article focuses on the mathematical formulation and practical implementation of the Fourier model fitting approach for vibration analysis in the context of an enhanced damping system for car wheel suspension. The methodology involves calculating the Fourier coefficients from the experimental data, reconstructing the signal using a truncated Fourier series representation, and validating the model's accuracy.

2. Methodology and Information-technical support

Modifying the template – including but not limited to: adjusting margins, typeface sizes, line spacing, paragraph and list definitions – is not allowed.

Fourier model fitting approach for vibration analysis of an enhanced damping system for car wheel suspension involves the following steps.

Data Acquisition: We have the results of an experiment with the car's suspension system. The data were recorded using an accelerometer in two channels ("channel6" and "channel7") placed at two different control bumps. The experiment was repeated for various wheel rotation frequencies and different tire pressures. The vibration data obtained from the accelerometers often contains various types of noise and artifacts that can adversely affect the subsequent analysis and model fitting processes. Therefore, it is essential to preprocess the raw data before applying the Fourier model fitting technique. The data preprocessing steps involve detrending and normalization.

Data Preprocessing: Apply necessary preprocessing steps to the acquired data to remove potential biases or unwanted components of the signal.

In order to conduct experimental study aimed at confirming the results of theoretical studies and refining the corresponding parameters, a test stand with a drive drum was designed and manufactured for the experimental investigation of the shock absorber of a wheeled vehicle. The design scheme and overall appearance of the stand are shown in Figure 1. The essence of the test stand with the drive drum is the ability to conduct research under static load of the object under study (pneumatic shock absorber of a wheeled vehicle) and to record changes over time in the speed of movement and the critical steering angle under identical parameters and critical values of the dynamic turning angle for the elastic characteristics of the shock absorbers for small longitudinal-angular vibrations [27, 28].

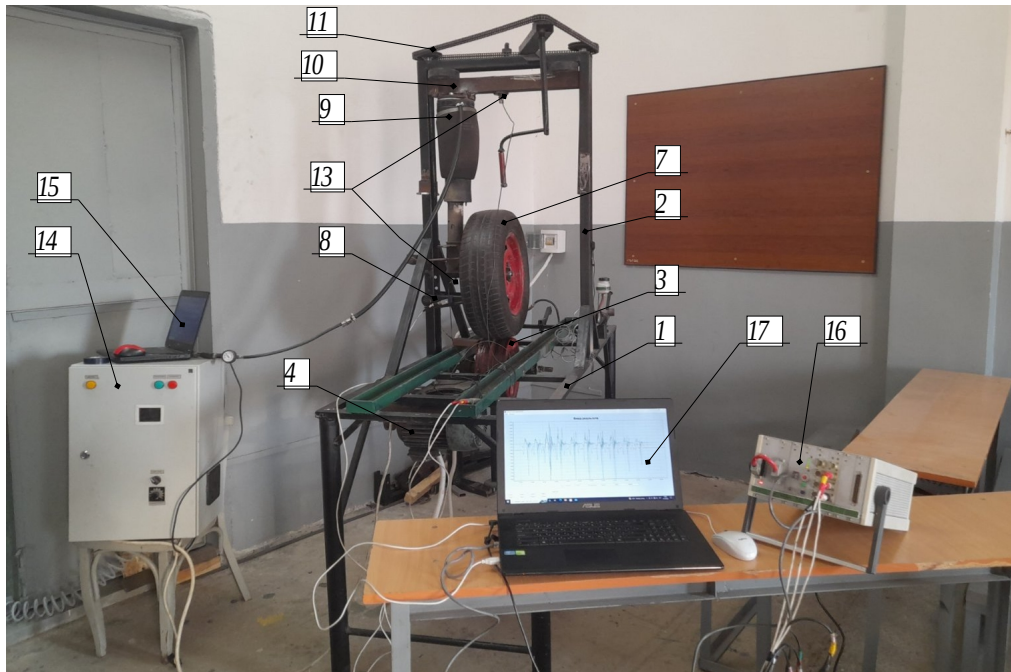


Figure 1: A stand with a drive drum for studying the car suspension with experimental equipment for fixing the studied characteristics under static load [29] (<https://ceur-ws.org/Vol-3628/paper29.pdf>).

During the experiment, the variable parameters were the rotational speed of the motor shaft (drive drum), the pressure in the chamber of the adjustable pneumatic shock absorber, and the height of the load on the drive drum (simulation of the wheel hitting an obstacle or entering a pothole).

The range of the electric motor shaft rotational speed change was 10Hz, 20Hz, 30Hz, and 40Hz, corresponding to the speed of the wheel movement of 15 km/h, 30 km/h, 45 km/h, and 60 km/h, respectively.

The pressure in the pneumatic chamber of the active type shock absorber was varied in the range of 1 atm, 1.5 atm, 2 atm, and 2.5 atm for each of the values of the electric motor shaft rotation frequency of the drive drum. The main technical parameters of the universal recording system (accelerometer 16) include the sampling frequency ranging from 1 Hz to 2 kHz per channel and an error in measurement values of no more than 4% (1% - due to accelerometer specifications and up to 3% - due to installation errors) [29].

The experimental data were recorded using a special digital measuring system, whose universal measuring channels allow us to connect the resistive sensors and sensors with output signals in the form of direct current voltage. The digital data of the experimental research are stored as binary files with the ".dat" extension.

3. Theoretical Background

Let $f(t)$ be a periodic function with period T , representing the vibration signal from the suspension system. According to the Fourier series theory, $f(t)$ can be expressed as an infinite sum of sinusoidal terms with different frequencies, amplitudes, and phases:

$$f(t) = a_0 + \sum_{n=1}^{\infty} \left[a_n \cos\left(\frac{2\pi nt}{T}\right) + b_n \sin\left(\frac{2\pi nt}{T}\right) \right], \quad (1)$$

where a_0 is the constant term (DC component), and a_n and b_n are the Fourier coefficients for the cosine and sine terms, respectively, at the n -th harmonic frequency $\frac{n}{T}$.

The Fourier coefficients can be calculated from the experimental data using the following integrals:

$$a_0 = \frac{1}{T} \int_0^T f(t) dt, \quad (2)$$

$$a_n = \frac{2}{T} \int_0^T f(t) \cos\left(\frac{2\pi nt}{T}\right) dt \text{ for } n \geq 1, \quad (3)$$

$$b_n = \frac{2}{T} \int_0^T f(t) \sin\left(\frac{2\pi nt}{T}\right) dt \text{ for } n \geq 1, \quad (4)$$

In practice, these integrals were approximated using Matlab built-in integration technique (`fft()` and `ifft()`) based on the discrete samples of the vibration signal.

3.1. Detrending

The detrending step aims to remove any underlying linear trend present in the vibration signal, as described in the context. This linear trend can arise due to various factors, such as sensor drift, gradual changes in the system's behavior over time, or other slowly varying environmental conditions. Taking into account for this trend can introduce biases in the subsequent Fourier analysis and model fitting processes.

To remove the linear trend, we employed polynomial regression using a first-order polynomial (i.e., a straight line). Let $\chi(t)$ denote the raw vibration signal obtained from the accelerometer at time t . We can model the linear trend as:

$$p(t) = a_1 t + a_0, \quad (5)$$

where a_1 and a_0 are the coefficients of the first-order polynomial that represent the slope and the intercept, respectively.

The coefficients a_1 and a_0 can be estimated using the method of least squares, which minimizes the sum of squared residuals between the observed data points and the fitted polynomial. Mathematically, we aim to find the values of a_1 and a_0 that minimize the following objective function:

$$J(a_1, a_0) = \sum_{i=1}^N [x(t_i) - (a_1 t_i + a_0)]^2, \quad (6)$$

where N is the total number of data points, and t_i and $x(t_i)$ are the time and the corresponding vibration signal value for the i -th data point, respectively.

By setting the partial derivatives of $J(a_1, a_0)$ with respect to a_1 and a_0 to zero, we obtain the normal equations:

$$\sum_{i=1}^N [x(t_i) - (a_1 t_i + a_0)] = 0, \quad (7)$$

$$\sum_{i=1}^N t_i [x(t_i) - (a_1 t_i + a_0)] = 0. \quad (8)$$

These equations can be solved simultaneously to find the least-squares estimates of a_1 and a_0 , denoted as \hat{a}_1 and \hat{a}_0 , respectively.

Once the coefficients \hat{a}_1 and \hat{a}_0 are determined, the detrended vibration signal $x_{\text{detrended}}(t)$ can be obtained by subtracting the fitted linear trend from the original signal:

$$x_{\text{detrended}}(t) = x(t) - (\hat{a}_1 t + \hat{a}_0). \quad (9)$$

The detrended signal $x_{\text{detrended}}(t)$ is now free from the linear trend and can be used as input for the subsequent normalization step and Fourier model fitting procedure.

3.2. Normalization

After detrending the vibration signal to remove the linear trend, the next step in data preprocessing is normalization. Normalization is a crucial step that ensures the vibration data from different experimental conditions or setups are brought to a common scale, allowing for a fair comparison and reliable analysis.

In our study, we employed z-score normalization, also known as standard score normalization, to standardize the detrended vibration signal. The z-score normalization process involves subtracting the mean value from the signal and dividing by the standard deviation, transforming the data to have a mean of zero and a unit standard deviation.

Let $x_{\text{detrended}}(t)$ denote the detrended vibration signal obtained after removing the linear trend. The z-score normalization is performed as follows:

$$x_{\text{normalized}}(t) = \frac{x_{\text{detrended}}(t) - \mu}{\sigma}, \quad (10)$$

where μ and σ are the mean and standard deviation of the detrended vibration signal $x_{\text{detrended}}(t)$, respectively.

The mean μ is calculated as:

$$\mu = \frac{1}{N} \sum_{i=1}^N x_{\text{detrended}}(t_i), \quad (11)$$

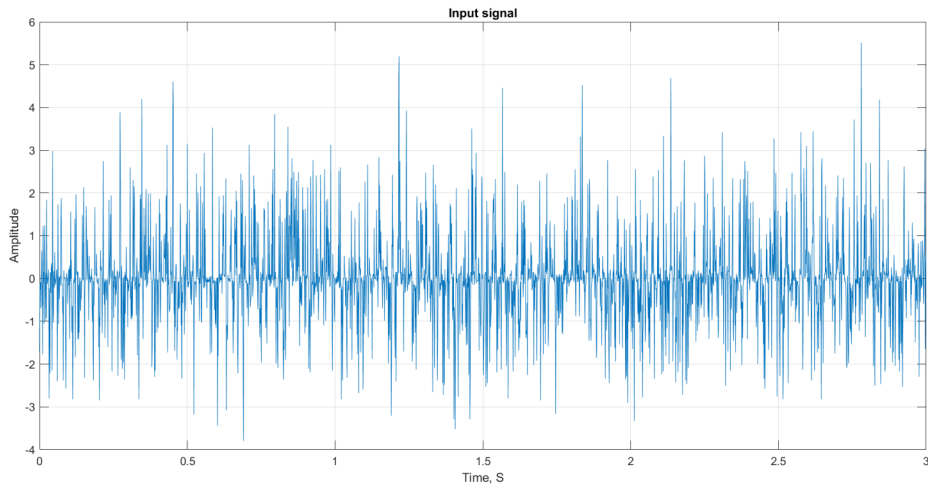
where N is the total number of data points, and t_i and $x_{\text{detrended}}(t_i)$ are the time and the corresponding detrended vibration signal value for the i -th data point, respectively.

The standard deviation σ is calculated as:

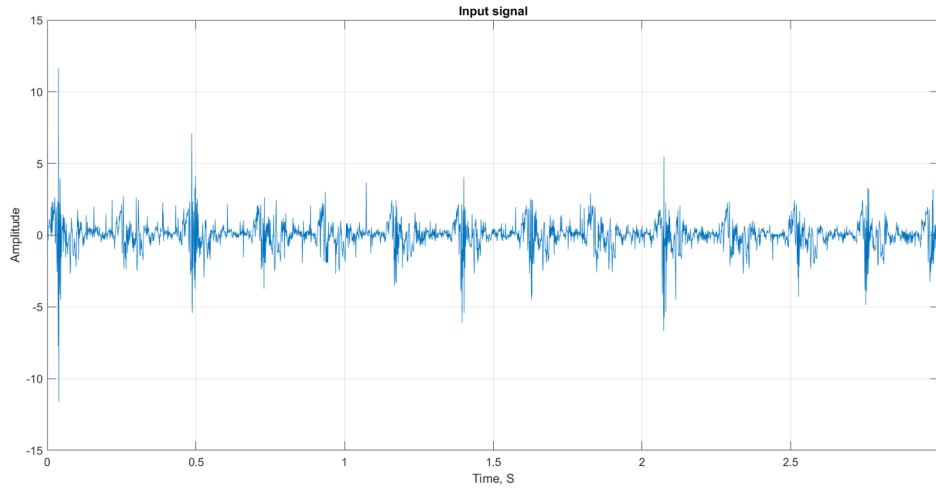
$$\sigma = \sqrt{\frac{1}{N} \sum_{i=1}^N [x_{\text{detrended}}(t_i) - \mu]^2}. \quad (12)$$

By subtracting the mean μ from the detrended signal and dividing by the standard deviation σ , we obtain the normalized vibration signal $x_{\text{normalized}}(t)$, which has a mean of zero and a standard deviation of one.

The z-score normalization ensures that the vibration data from different experimental conditions or setups, which may have different amplitudes or offsets, are brought to a common scale. This normalization step is crucial for ensuring that the subsequent Fourier analysis and model fitting are not unduly influenced by differences in the signal amplitudes or offsets, allowing for a more reliable and accurate analysis.



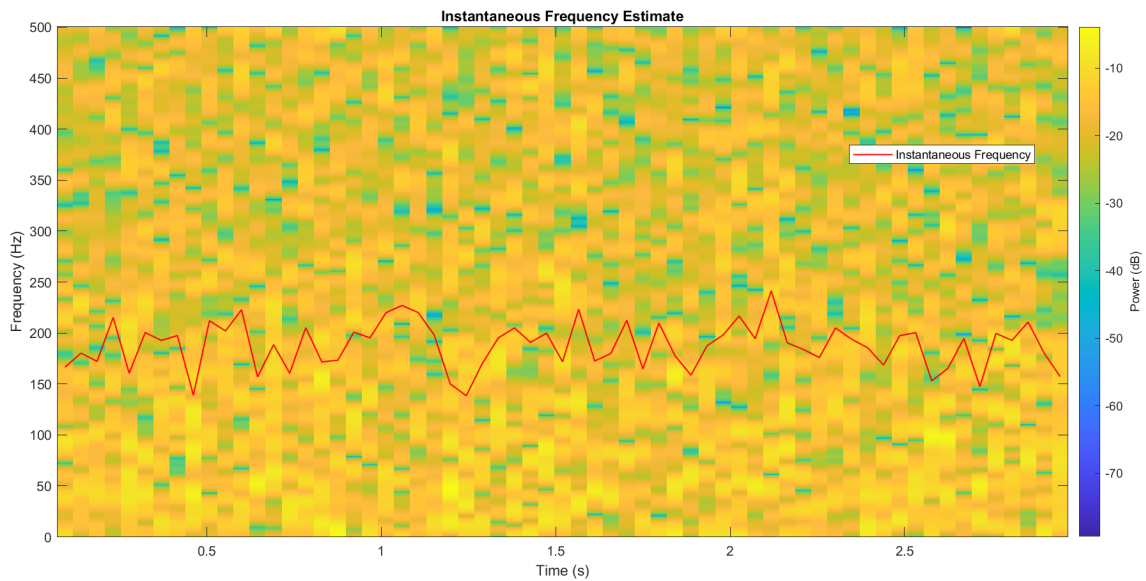
a)



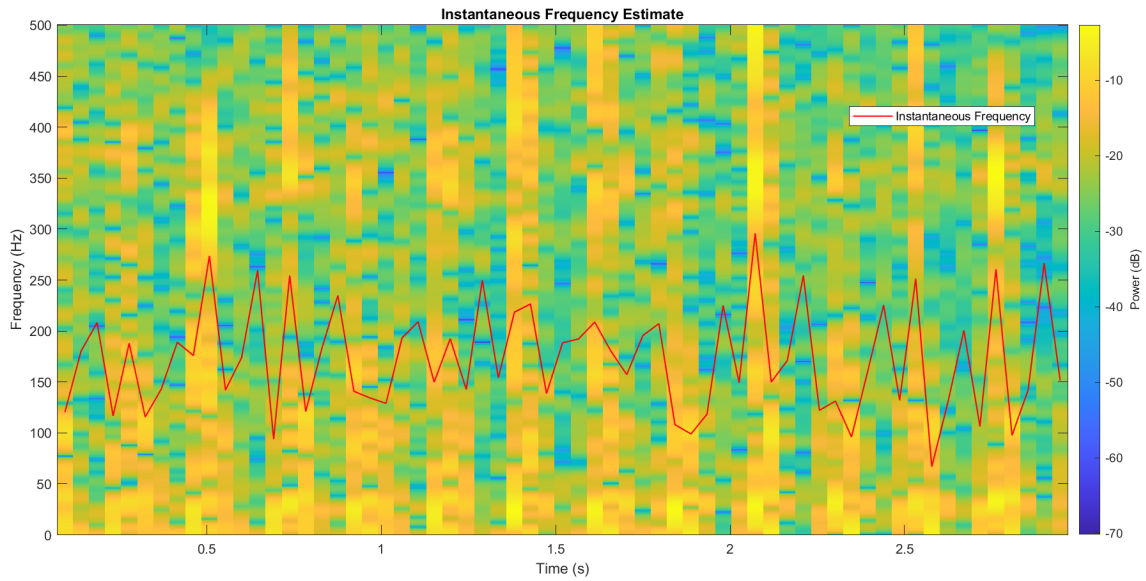
b)

Figure 2: Detrended and normalized signal plot for "channel6" (a) and "channel7" (b) (10 Hz, 1.0 atm)

After applying the detrending and normalization steps, the preprocessed vibration signal $x_{\text{preprocessed}}(t) = x_{\text{normalized}}(t)$ is ready for the Fourier model fitting procedure, where the periodic components and their corresponding amplitudes and phases can be accurately estimated (Figure 2 and Figure 3).



a)

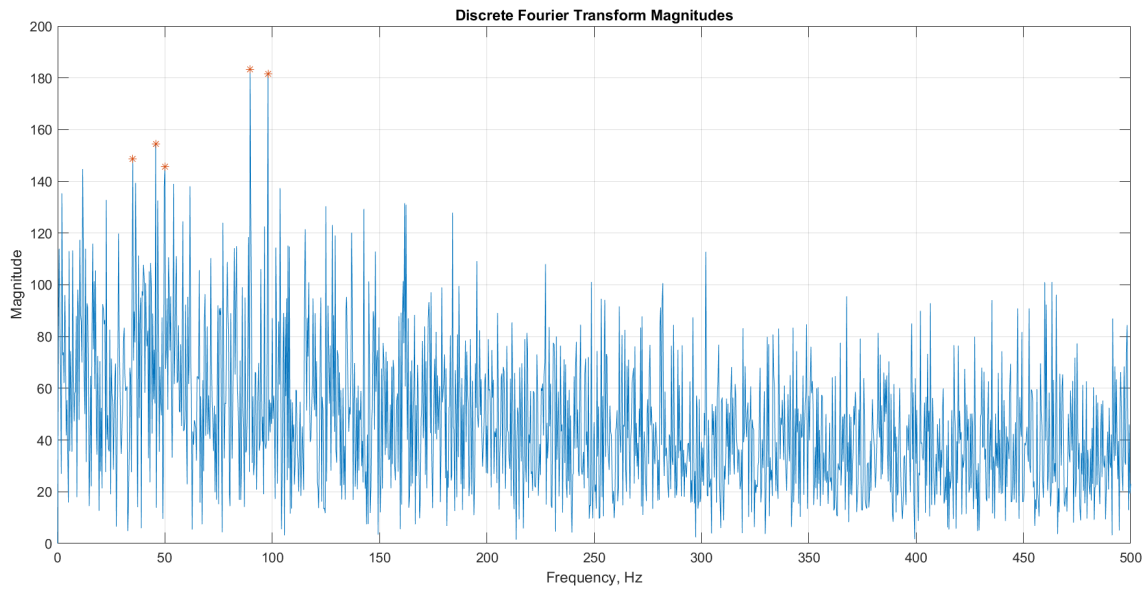


b)

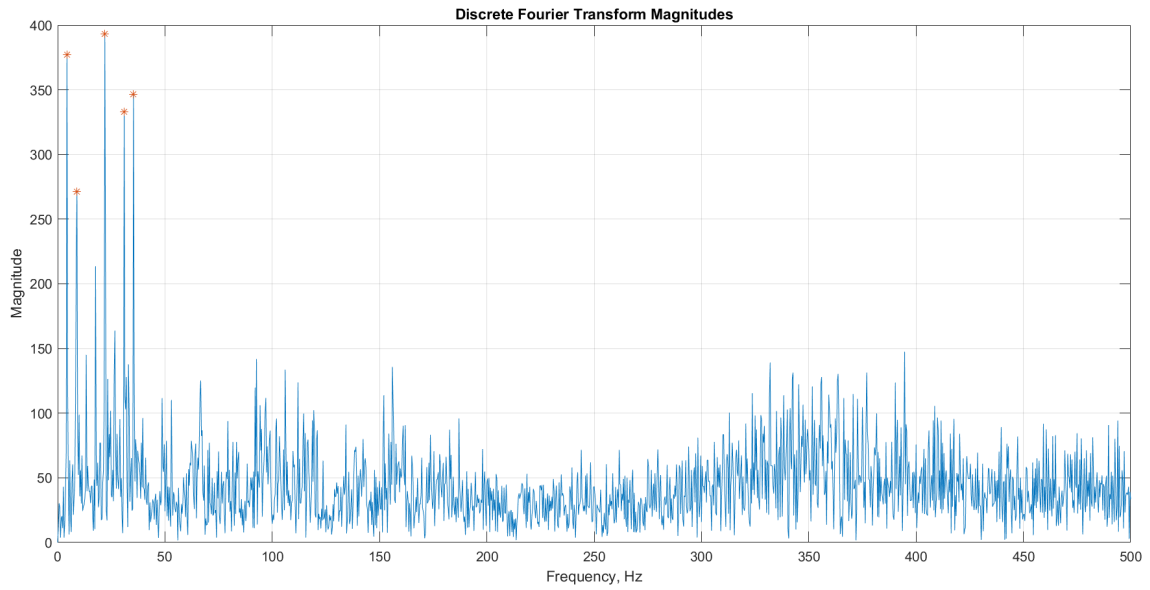
Figure 3: Power spectrogram and instantaneous frequency estimate of "channel6" (a) and "channel7" (b) signal plot (10 Hz, 1.0 atm)

3.3. Fourier Coefficient Calculation

Calculate the Fourier coefficients (a_0 , a_n , and b_n) as mentioned previously in chapter "Theoretical Background" from the preprocessed vibration data using Fast Fourier Transform (FFT) algorithm (Figure 4).



a)

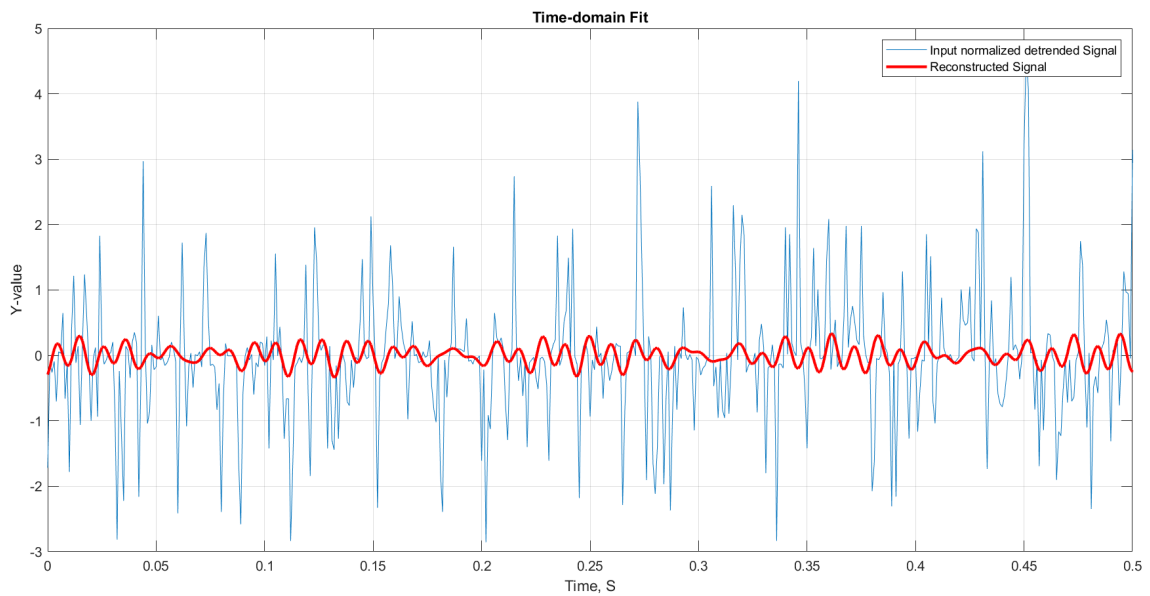


b)

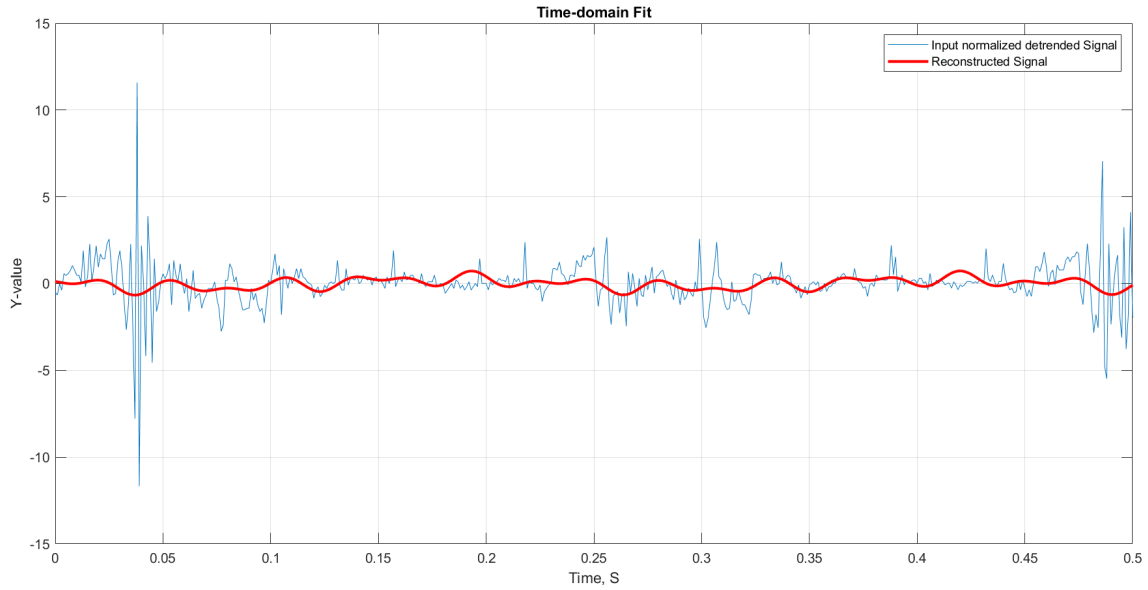
Figure 4: Discrete Fourier transform magnitudes plot of "channel6" (a) and "channel7" (b) (10 Hz, 1.0 atm)

3.4. Truncated Fourier Series Representation

Was reconstructed the vibration signal using a truncated Fourier series representation by considering only 5 the most significant harmonic components (Figure 5).



a)



b)

Figure 5: Five the most significant harmonic time-domain fit of "channel6" (a) and "channel7" (b) (10 Hz, 1.0 atm)

The number of harmonics retained in the model can be determined based on the desired accuracy or signal energy preservation criteria. Model is in the form:

$$f(x) = a_0 + a_1 \cdot \cos(x \cdot w) + b_1 \cdot \sin(x \cdot w) + a_2 \cdot \cos(2 \cdot x \cdot w) + b_2 \cdot \sin(2 \cdot x \cdot w) + a_3 \cdot \cos(3 \cdot x \cdot w) + b_3 \cdot \sin(3 \cdot x \cdot w)$$

The fundamental frequency, F , derived from the Fourier model fit, is calculated

$$F = 1 / (2 * \pi / w) = 55.00 \text{ Hz.}$$

It is important to note that this fundamental frequency should not necessarily coincide with the lower harmonic component that exhibits a large amplitude in the Fourier spectrum. The fundamental frequency represents the base frequency or the period of the signal, while the lower harmonic with a large amplitude may correspond to a specific vibration mode or resonance frequency of the system.

It is worth mentioning that the fundamental frequency may correlate with the main period of the autocorrelation function of the vibration signal.

However, a detailed exploration of the relationship between the fundamental frequency from the Fourier model fit and the autocorrelation function is beyond the scope of this article and could be a topic for future investigations. Such an analysis could involve comparing the fundamental frequency obtained from the Fourier model fit with the main period identified by the autocorrelation function, and examining the potential correlations or discrepancies between these two quantities.

3.5. Model Validation

Assess the accuracy of the truncated Fourier series model by comparing it with the original vibration data is necessary. To perform it we calculate these goodness-of-fit statistics for parametric models:

- The sum of squares due to error (SSE)
- R-square
- Degrees of freedom for error (DFE)
- Adjusted R-square
- Root mean squared error (RMSE).

The obtained results and quality metrics are summarized in the table 1.

Table 1
Goodness-of-fit statistics calculate results

		10 Hz, 1.0 atm		20 Hz, 1.5 atm	
		channel6	channel7	channel6	channel7
Most prominent peaks [Frequency, Amplitude]	f1	[89.67 183.40]	[22.00 393.16]	[21.33 168.86]	[9.00 441.94]
	f2	[98.00 181.57]	[4.33 377.20]	[49.67 161.52]	[98.67 334.45]
	f3	[45.67 154.46]	[35.33 346.71]	[98.67 160.21]	[27.00 277.18]
	f4	[35.00 148.78]	[31.00 332.94]	[5.33 149.07]	[18.00 265.45]
	f5	[50.00 145.63]	[9.00 271.12]	[104.33 146.23]	[349.67 263.26]
Coefficients (with 95% confidence bounds)	a0	0.0002957 (-0.03528, 0.03587)	-0.003516 (-0.03685, 0.02982)	0.0002837 (-0.03522, 0.03579)	2.239e-06 (-0.03412, 0.03412)
	a1	0.01924 (-0.03111, 0.06959)	0.2241 (0.1764, 0.2718)	0.08165 (0.03143, 0.1319)	0.2707 (0.2215, 0.3199)
	b1	-0.00692 (-0.05725, 0.04341)	-0.157 (-0.2052, -0.1089)	-0.01216 (-0.06326, 0.03895)	-0.1197 (-0.1719, -0.06743)
	a2	0.03073 (-0.01976, 0.08121)	0.1045 (0.05308, 0.156)	-0.05472 (-0.1053, -0.004102)	-0.08131 (-0.1355, -0.02717)
	b2	-0.01834 (-0.06918, 0.0325)	0.2371 (0.189, 0.2852)	0.02559 (-0.0264, 0.07758)	0.1649 (0.115, 0.2148)
	a3	-0.05469 (-0.1117, 0.002316)	-0.0004867 (-0.04928, 0.04831)	0.05545 (0.003424, 0.1075)	0.002528 (-0.06366, 0.06871)
	b3	-0.07799 (-0.1317, -0.02425)	0.09002 (0.0429, 0.1371)	0.0385 (-0.01534, 0.09234)	0.2005 (0.1523, 0.2488)

	a4	0.05908 (0.008446, 0.1097)	0.04055 (-0.01189, 0.09298)	0.03928 (-0.01976, 0.09832)	-0.002941 (-0.05708, 0.0512)
	b4	0.01293 (-0.04418, 0.07005)	0.1296 (0.08201, 0.1772)	0.06776 (0.01459, 0.1209)	0.08305 (0.03478, 0.1313)
	a5	-0.1308 (-0.1819, -0.07983)	-0.2829 (-0.3383, -0.2276)	0.05438 (-0.02916, 0.1379)	-0.1081 (-0.1683, -0.04789)
	b5	0.01485 (-0.0754, 0.1051)	0.1295 (0.0507, 0.2083)	0.1143 (0.05463, 0.174)	-0.09473 (-0.1576, -0.03182)
	w	112.8 (112.7, 112.9)	27.78 (27.75, 27.81)	26.71 (26.63, 26.79)	56.4 (56.35, 56.45)
goodness-of-fit model	sse	2951.276954	2588.078899	2935.356104	2714.102773
	rsquare	0.015876808	0.135464561	0.018658141	0.094893276
	dfe	2988	2988	2988	2988
	adjrsquare	0.012253864	0.132281867	0.015045437	0.091561223
	rmse	0.993835914	0.930675882	0.991151634	0.953065717
Fundamental	F	17.95	4.42	4.25	8.98

Continuation of the table 1

		30Hz 2,0 atm		40Hz 2,5 atm	
		channel6	channel7	channel6	channel7
Most prominent peaks	f1	[38.33 278.35]	[89.33 698.00]	[46.33 352.16]	[14.00 400.13]
	f2	[127.67 231.44]	[12.67 681.48]	[45.67 332.57]	[353.67 246.42]
	f3	[166.00 188.78]	[127.67 547.66]	[47.00 255.54]	[28.33 236.46]
	f4	[8.67 152.77]	[115.00 455.89]	[28.33 247.32]	[338.33 194.35]
	f5	[88.67 150.46]	[51.00 293.33]	[159.67 242.69]	[99.00 176.03]
Coefficients (with	a0	-4.076e-05 (-0.03516, 0.03508)	4.416e-05 (-0.03375, 0.03384)	-0.0001873 (-0.03544, 0.03506)	6.365e-06 (-0.03495, 0.03496)
	a1	-0.0362 (-0.08595, 0.01356)	-0.2975 (-0.3712, -0.2239)	0.2435 (0.1937, 0.2934)	0.06825 (0.003855, 0.1326)

95% confidence bounds)	b1	-0.0185 (-0.06831, 0.03131)	-0.3604 (-0.4269, -0.2938)	0.001561 (-0.07196, 0.07508)	0.2569 (0.2062, 0.3076)
	a2	-0.04618 (-0.09767, 0.005316)	0.02085 (-0.02704, 0.06873)	0.003764 (-0.04608, 0.05361)	-0.1324 (-0.1879, -0.07688)
	b2	0.06365 (0.0129, 0.1144)	0.009607 (-0.03862, 0.05783)	-0.001092 (-0.05098, 0.04879)	-0.07789 (-0.1431, -0.01268)
	a3	-0.1155 (-0.1851, -0.04598)	-0.02309 (-0.07483, 0.02865)	-0.05131 (-0.1169, 0.01428)	0.004898 (-0.04506, 0.05486)
	b3	-0.1457 (-0.2087, -0.08274)	0.04247 (-0.006528, 0.09148)	0.06407 (0.003613, 0.1245)	-0.01584 (-0.06532, 0.03365)
	a4	-0.04151 (-0.09561, 0.01259)	-0.04139 (-0.09222, 0.00944)	0.002392 (-0.04843, 0.05322)	0.02226 (-0.03014, 0.07466)
	b4	0.04885 (-0.004314, 0.102)	-0.02786 (-0.08216, 0.02643)	-0.01115 (-0.06105, 0.03875)	0.0266 (-0.0248, 0.078)
	a5	-0.08557 (-0.1369, -0.03422)	-0.003729 (-0.05183, 0.04437)	-0.02202 (-0.07963, 0.03559)	0.0157 (-0.05295, 0.08436)
	b5	-0.02381 (-0.09265, 0.04502)	-0.007047 (-0.05493, 0.04084)	0.02599 (-0.02953, 0.08152)	0.05895 (0.007863, 0.11)
	w	80.26 (80.18, 80.33)	561.4 (561.3, 561.5)	291.4 (291.2, 291.5)	87.99 (87.88, 88.09)
goodness-of-fit model	sse	2875.9296	2663.127549	2897.323267	2848.563685
	rsquare	0.02758774	0.11194364	0.033711847	0.049747535
	dfe	2988	2988	2988	2988
	adjrsquare	0.024007909	0.108674356	0.030154562	0.046249283
	rmse	0.981067364	0.944073239	0.984709619	0.976388533
Fundamental	F	12.77	89.35	46.37	14

Additionally, to investigate the mutual influences of two signals (“channel6” and “channel7”) obtained from different key points of the laboratory setup, a cross-spectrogram was constructed.

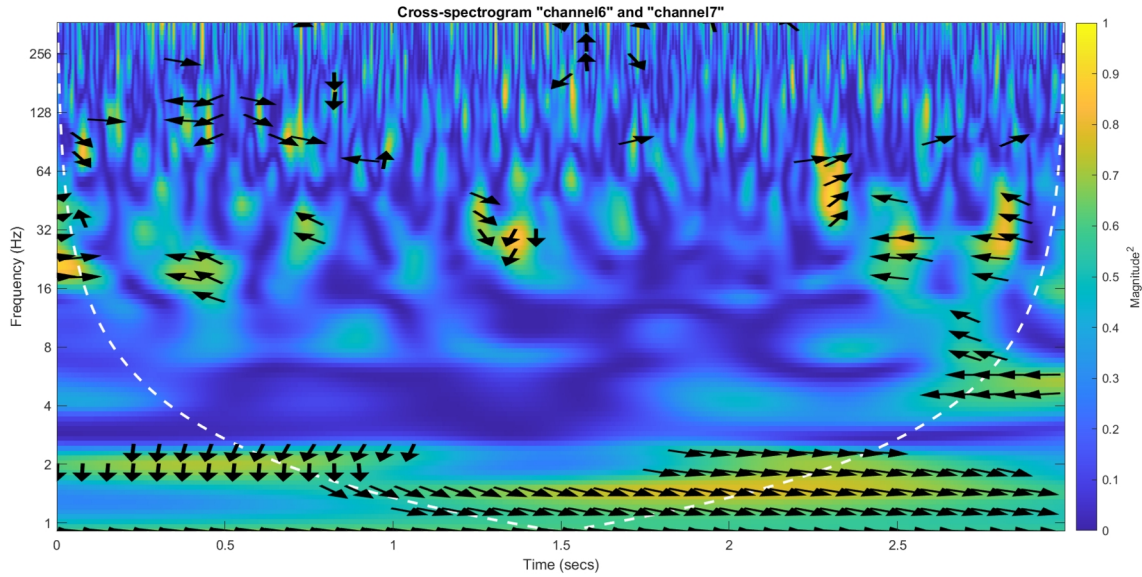


Figure 6: Cross-spectrogram of "channel6" and "channel7" (10 Hz, 1.0 atm)

Cross-spectrogram is a powerful tool for analyzing the time-frequency relationships between two nonstationary signals. It provides a measure of the correlation between two signals in the time-frequency plane, allowing researchers to identify common patterns and oscillations that are localized in both time and frequency. Here, we will delve into the details of interpreting cross-spectrogram plot results, focusing on the key aspects to consider when analyzing the mutual influences of two signals.

A cross-spectrogram plot consists of a two-dimensional representation of the time-frequency plane, where the x-axis represents time and the y-axis represents frequency. The color scheme used in the plot indicates the magnitude of the coherence between the two signals, with higher coherence values (closer to 1) indicating stronger correlations and lower values (closer to 0) indicating weaker correlations. One of the primary goals of cross-spectrogram analysis is to identify coherent oscillations between the two signals. These oscillations are characterized by high coherence values in specific regions of the time-frequency plane. Coherence values range from 0 to 1 and indicate the strength of the correlation between the two signals at a given time and frequency. Strong correlation (close to 1) between the two signals, indicating that they share common oscillations or patterns. Weak correlation between the two signals, suggesting that they do not share common oscillations or patterns. The phase of the cross-spectrum provides information about the relative lag between the two signals. The phase is plotted against frequency to identify the lag at different frequencies.

The results demonstrate the effectiveness of the Fourier model fitting technique in capturing the dominant vibration patterns and identifying the critical frequencies associated with the suspension system's performance. By analyzing the magnitudes of the Fourier coefficients, it becomes possible to pinpoint the frequencies that contribute significantly to the overall vibration behavior.

4. Computer modeling

The obtained results of experimental studies of the load on the active type shock absorber were used to investigate the stress-strain state (SSS) of the elements of this shock absorber in a static problem statement by means of computer modeling.

Modeling of the active type shock absorber was carried out using the tools of the SOLIDWORKS three-dimensional modeling system, which makes it possible to carry out the engineering analysis of a wide variety of designs with a large number of different parameters [30].

The study of the stress-strain state (SSS) of an automotive shock absorber CAD model (Figure 7) was carried out in the SolidWorks Simulation engineering analysis module, where only the rubber element was investigated in the first stage. Other elements of the model were excluded from the analysis.

The rubber element was fixed between the cover and the body of the shock absorber (Figure 7). The load applied was an internal pressure of 1.5 atm (0.151 MPa) and a displacement of 20 mm of the rubber element (turnover of the rubber element that rests against the shock absorber).

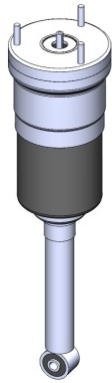


Figure 7: CAD-model of a shock absorber

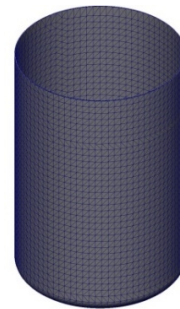


Figure 8: Mesh of finite elements

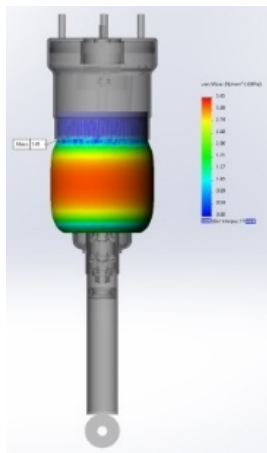


Figure 9: Distribution of normal stresses

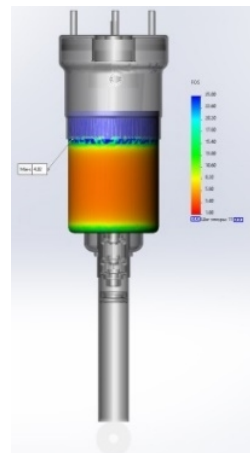


Figure 10: Distribution of safety margin

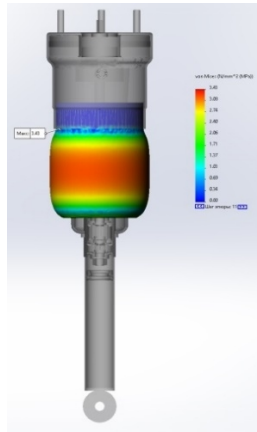


Figure 11: Distribution of normal stresses

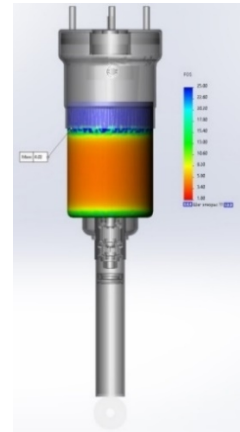


Figure 12: Distribution of safety margin

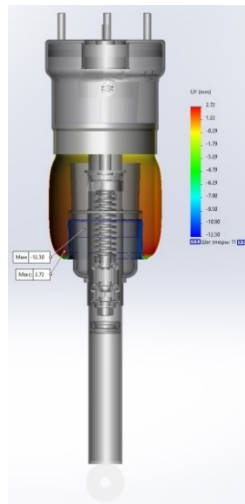


Figure 13: Axial displacement of the rubber element

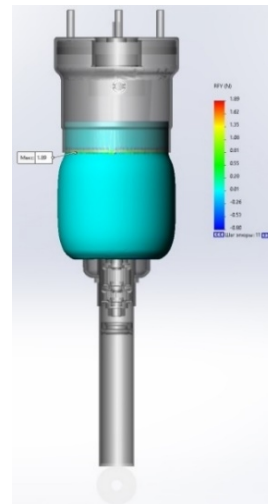


Figure 14: Axial force on the rubber element

The finite element mesh was standard with a check for distorted elements. The global size of the finite elements was 5 mm with a tolerance of 0.25 mm (Figure 8). As a result of the calculation, the maximum stress of 3.43 MPa is observed near the fixation point (Figure 9), the minimum safety factor is ≈ 4 (Figure 10), the maximum deformation of the rubber element is 0.11 (11%) (Figure 11), and the maximum resulting displacement is 12.31 mm (Figure 12). The axial (vertical) displacement of the rubber element is as follows: lower edge of the outer cylinder - 2.72 mm (upward); rubber element - 12.3 mm (downward) (Figure 13). The axial force on the rubber element is 1.89 N (Figure 14).

Conclusion

This article presented a comprehensive mathematical framework for vibration analysis of an enhanced damping system for car wheel suspension using the Fourier model fitting approach. The methodology involves calculating the Fourier coefficients from experimental data, reconstructing the vibration signal using a truncated Fourier series representation, and validating the model's accuracy.

The Fourier model fitting technique provides valuable insights into the dynamic behavior of the suspension system by identifying the dominant frequencies contributing to the vibration patterns. This information can guide the optimization process by suggesting potential modifications to the damping system or adjustments to the suspension parameters to mitigate or enhance specific vibration modes, ultimately improving ride comfort and handling characteristics.

Future work may involve investigating advanced signal processing techniques, such as time-frequency analysis or wavelet transforms, to capture non-stationary or transient vibration phenomena. Additionally, incorporating numerical simulations or finite element models could complement the experimental data analysis and facilitate a more comprehensive understanding of the suspension system's dynamics.

References

- [1] Gysen B. L. J., Paulides J. J. H., Janssen J. L. G., Lomonova E. A. Active electromagnetic suspension system for improved vehicle dynamics. *IEEE Transactions on Vehicular Technology*. 2010. 59(3):1156-1163. <https://doi.org/10.1109/TVT.2009.2038706>.
- [2] Martins I., Esteves M., Pina da Silva F., Verdelho P. Electromagnetic hybrid active-passive vehicle suspension system. *IEEE 49th Vehicular Technology Conference (Cat. No.99CH36363)*, Houston, TX, USA, 1999, vol.3, 2273-2277. doi: 10.1109/VETEC.1999.778470.
- [3] Bello M. M., Babawuro A. Y., Fatai S. Active suspension force control with electro-hydraulic actuator dynamics. *ARPJ Journal of Engineering and Applied Sciences*. 2015. 10(23):17327-17331. ISSN 1819-6608.
- [4] Rosli R., Mailah M., Priyandoko G. Active suspension system for passenger vehicle using active force control with iterative learning algorithm. *WSEAS Transactions on Systems and Control*. 2014. 9(2):120-127. E-ISSN: 2224-2856.
- [5] Moheyeldin M. M., El-Tawwab A. M. A., El-gwwad K. A. A., Salem M. M. M. An analytical study of the performance indices of air spring suspensions over the passive suspension. *Beni-Suef University Journal of Basic and Applied Sciences*. 2018. 7(4): 525-534. <https://doi.org/10.1016/j.bjbas.2018.06.004>.
- [6] Shafie M., Bellob M., Khan R. M. "Active vehicle suspension control using electro hydraulic actuator on rough road terrain". *Journal of Advanced Research in Applied Mechanics*. 2015. 9(1): 15-30. ISSN (online): 2289-7895.
- [7] Artiushenko A., Suiarkov O. Study of the influence of the characteristics of the small-sized car suspension on driving qualities and its modernization. *Bulletin of NTU "KHPI"*.2013. 31(1004): 21-27. [in Ukrainian].

- [8] Petraška A., Čižiūnienė K., Jarašūnienė A., Maruschak P. & Prentkovskis O. Algorithm for the assessment of heavyweight and oversize cargo transportation routes. *Journal of Business Economics and Management*. 2017. 18. 1098-1114. 10.3846/16111699.2017.1334229.
- [9] Derbaremdyker A. D., Musarskyi P. A., Stepanov I. O., Yudkevych M. A. Self-adjusting shock absorber with programmed damping characteristic. *Automotive industry*. 1985. 1: 13 – 15. [in Russian].
- [10] Audi Technology Portal: Dynamic Ride Control. URL: https://www.audi-technology-portal.de/en/chassis/suspension-controlsystems/dynamic-ride-control_en.
- [11] Sim K., Lee H., Yoon J. W., Choi C., Hwang S. H. Effectiveness evaluation of hydropneumatic and semi-active cab suspension for the improvement of ride comfort of agricultural tractors. *Journal of Terramechanics*. 2017. 69: 23-32. <https://doi.org/10.1016/j.jterra.2016.10.003>.
- [12] Guiggiani M. The science of vehicle dynamics. Dordrecht: Springer Netherlands. 2014. 130.
- [13] Ingle V. K., & Proakis J. G. Digital Signal Processing Using MATLAB (3rd ed.). Northeastern University. 2021. ISBN-13: 978-1-111-42737-5 https://www.academia.edu/44421125/Digital_Signal_Processing_Using_MATLAB_Third_Edition.
- [14] Elali T. S. Discrete Signals and Systems with Matlab(r). CRC Press. 2020. ISBN: 9780367539931. <https://www.mathworks.com/academia/books/discrete-signals-and-systems-with-matlab-elali.html>.
- [15] Asadi F. Signals and Systems with MATLAB® and Simulink®. In Synthesis lectures on engineering, science, and technology. 2024. <https://doi.org/10.1007/978-3-031-45622-0>. <https://link.springer.com/book/10.1007/978-3-031-45622-0>.
- [16] Quinquis A. Digital signal processing using Matlab. Wiley-ISTE. 2008. <https://onlinelibrary.wiley.com/doi/pdf/10.1002/9780470610992.fmatter>.
- [17] Pan H., Sun W., Jing X., Gao H., Yao J. Adaptive tracking control for active suspension systems with non-ideal actuators. *Journal of Sound and Vibration*. 2017. 399, 2-20. <https://doi.org/10.1016/j.jsv.2017.03.011>.
- [18] Popular Mechanics: 3 Technologies That Are Making Car Suspensions Smarter Than Ever. URL: <https://www.popularmechanics.com/cars/car-technology/a14665/why-car-suspensions-are-better-than-ever>.
- [19] Jazar R. N. Vehicle dynamics. New York: Springer New York: 2014. 396.
- [20] Jazar R. N. Vehicle dynamics: theory and application. Boston: Springer US. 2008. 1015.
- [21] Mandryka V. R., Shlykova V. H. Controllability and stability of the car in class B with the system ESP. *Bulletin of NTU "KHPI"*. 2013. 31(1004). 60-65. [in Ukrainian].
- [22] Pavlenko V. M., Kryvoruchko O. O. The current state of passenger cars active suspensions development. *Automotive industry*, 2014. 9(1052): 54-60. [in Ukrainian].
- [23] Popp K., Schiehlen W. "Ground vehicle dynamics". Berlin; Heidelberg: Springer Berlin Heidelberg, 2010.396. <https://doi.org/10.1007/978-3-540-68553-1>.
- [24] Schramm D., Hiller M., Bardini R. Vehicle dynamics. Berlin, Heidelberg: Springer Berlin Heidelberg, 2018.:433. DOI 10.1007/978-3-662-54483-9.
- [25] Taghavifar H., Mardani A. Off-road vehicle dynamics. Cham: Springer International Publishing, 2016. 396.
- [26] Hevko B., Hevko R., Klendii O., Buriak M., Dzyadykevych Y. & Rozum R. Improvement of machine safety devices. *Acta Polytechnica*. 2018. 58. 17. 10.14311/AP.2018.58.0017.

- [27] A stand for researching the characteristics of a car's suspension: Patent 148601, Ukraine: G01N 17/00 (2021.01). № u202101835; stat. 07.04.21; publ. 26.08.21, Bul. 34. [in Ukrainian].
- [28] A stand for researching the characteristics of a car's suspension: Patent 150771 Ukraine: G01N 3/00, F16D 65/00. № u202106434; stat. 15.11.21; publ. 13.04. 22, Bul. 15. [in Ukrainian].
- [29] Lyashuk O., Stashkiv M., Lytvynenko I., Sakhno V., Khoroshun R. Information Technologies Use in the Study of Functional Properties of Wheeled Vehicles. *The 3rd International Workshop on Information Technologies: Theoretical and Applied Problems 2023* (ITTAP 2023). Vol. 3628. 500-512.
- [30] Petrov O., Piontkevych O., Buda A. & Kolomiets V. Application of the CAD/CAE system Solidworks in the tasks of analysis of strength of parts of the clamping fixtures. *Journal of Mechanical Engineering and Transport*. 2024. 19. 95-102. 10.31649/2413-4503-2024-19-1-95-102.